Appl. Phys. B 46, 221–236 (1988)

Applied Physics B Photophysics and Laser Chemistry

Laser Spectroscopy for Studying Chemical Processes

J. Wolfrum

Physikalisch-Chemisches Institut, Universität, Im Neuenheimer Feld 253, D-6900 Heidelberg, Fed. Rep. Germany

Received 11 March/Accepted 15 March 1988

Abstract. In recent years, various methods have been developed to observe and to influence the course of chemical reactions using laser radiation. By selectively increasing the translational, rotational, and vibrational energies and by controlling the relative orientation of the reaction partners with tunable infrared and UV lasers, direct insight can be gained into the molecular course of the breaking and re-forming of chemical bonds. As examples for the application of lasers in chemical synthesis the production of monomers and catalysts is discussed. The application of linear and nonlinear laser spectroscopic methods, such as laser-induced fluorescence (LIF), Coherent anti-Stokes Raman Scattering (CARS), infrared-absorption measurements with tunable diode and molecular lasers is described for non-intrusive observation of the interaction of transport processes with chemical reactions used in industrial processes with high temporal, spectral and spatial resolution. Finally the application of a UV laser microbeam apparatus in genetic engineering for laser-induced cell fusion, genetic transformation of plant cells as well as diagnosis of human diseases by laser-microdissection of chromosomes is described.

PACS: 82.20, 82.30, 82.50, 82.80, 87

Irradiation with light can have a considerable influence on the course of chemical reactions. The best known example is the photosynthesis in plants by sunlight. In addition, electromagnetic radiation is the most important aid to determining structure, properties, and behaviour of chemically reacting substances. In spite of great successes, spectroscopy with conventional light sources has not been able to answer many interesting questions. As in other areas of science and technology, the laser has also created numerous new possibilities for the investigation of chemical processes. Particularly the introduction of tunable laser light sources, such as the dye laser [1] and the development of linear and nonlinear optical techniques such as laser-induced fluorescence (LIF), resonant multiphoton ionization (REMPI), coherent anti-Stokes Raman spectroscopy (CARS), laser Raman spectroscopy on surfaces (SERS), photoacoustic spectroscopy (PAS), laser magnetic resonance spectroscopy (LMR) and Doppler-free absorption spectroscopy, allow virtually every spectroscopic state of an atom or molecule to be observed with high resolution, from the far infrared with wavelengths of several millimetres to wavelengths in the nanometre range in the vacuum ultraviolet [2]. The high sensitivity makes observation of single atoms and molecules possible. Furthermore, laser spectroscopy can provide non-intrusive observation of rapidly changing chemical reactions, such as combustion processes, with high temporal, spectral, and spatial resolution. In this contribution the application of laser techniques to observe and to stimulate chemical reactions will be described in four different areas: chemical kinetics, chemical synthesis, industrial chemical reactors and genetic engineering.

1. Microscopic Dynamics of Elementary Chemical Reactions

The strong dependence of the rate of chemical reactions on the energy supplied is one of the most important observations for the chemist. Often, the

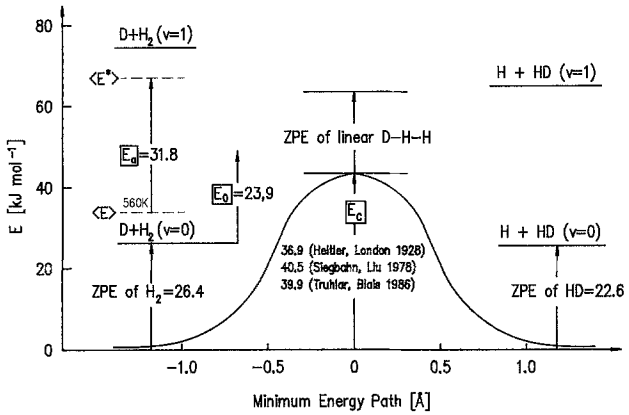

Fig. 1. Characteristic energy requirements of the hydrogen exchange reaction. E_a is the Arrhenius activation energy, E_0 the minimum collision energy that leads to reaction (threshold energy), and E_c the height of the potential energy barrier of the reaction in the vibrational ground state, $\langle E \rangle$ is the average thermal energy of all binary collisions per unit time and $\langle E^* \rangle$ the average kinetic energy of all collisions per unit time that lead to reaction. ZPE is the zeropoint energy of vibration

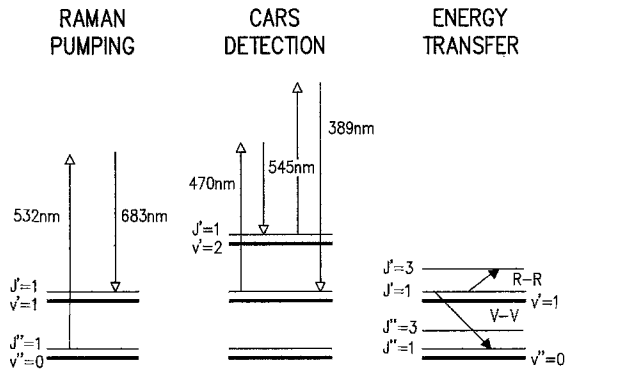

Fig. 2. Energy level diagram for the excitation and detection of state-selected hydrogen molecules by Raman and CARS spectroscopy

energy of the reaction partners can be represented by one temperature and the dependence of the reaction rate on temperature is described by the now nearly one-hundred-year-old Arrhenius equation [3]. The Arrhenius parameters obtained in this way do not, however, provide any information on the respective contribution of the degree of freedom of the participating reaction partners to overcoming the energy barrier of the reaction. In the following examples, reactions in the gas phase are used to show how information on microscopic details of breaking and re-forming of bonds in chemical reactions can be obtained in experiments with lasers. Such information can be used to influence chemical reactions much more selectively than by classical thermal heating of the reactants.

The reaction of hydrogen molecules with hydrogen atoms or their isotopes, as the simplest example of a bimolecular reaction of neutral particles, is particularly suitable for a theoretical investigation of the influence of selective excitation of reacting species. The energy of one vibrational quantum of the hydrogen molecule considerably exceeds the Arrhenius activation energy (E_a), the threshold energy (E_0) as well as the height of the potential energy barrier (E_c) of the reaction in the vibrational ground state (see Fig. 1). E_c was first calculated quantum mechanically by London [4] more than half a century ago. Classical methods for the study of reaction kinetics are difficult to apply to this reaction, because known concentrations of vibrationally excited hydrogen molecules have to be produced and detected. Due to the lack of a dipole moment and an electronic absorption spectrum in the vacuum ultraviolet, state-selective studies using spectroscopic methods were difficult to perform for a long time, before laser methods became available. Figure 2 shows the excitation and detection scheme of a laser experiment for energy transfer and state-selective reaction studies of hydrogen molecules. Stimulated Raman pumping is employed to populate H_2 ($v''=1$, $J''=1$) selectively in the electronic ground state of hydrogen within a 10 ns laser pulse. The time-dependent populations in rotational and vibrational levels in hydrogen and isotopic modifications can be probed by coherent anti-Stokes Raman spectroscopy (CARS). In the experimental arrangement [5] 50% of the energy output of a linearly polarized frequency-doubled Nd:YAG laser (Quanta Ray DCR1A, at 532 nm) is focussed into a Raman cell containing a hydrogen-helium mixture with partial pressures of 20 bar and 10 bar, respectively. The helium is used to reduce the pressure-dependent line shift of the Stokes line. Stimulated Stokes Raman radiation is generated in forward and backward directions. Due to the phase conjugation effect in stimulated Raman scattering, the backward beam displayed a more homogeneous intensity distribution over the beam cross section and a smaller divergence than the forward scattered beam. Both beams are focussed into the centre of the reaction cell with a beam waist of about 200 µm diameter for both fundamental and Stokes beams. The rate constants obtained from this experiment for the relaxation processes

$$H_2(v=1, J=1) \underset{k_{31}}{\overset{k_{13}}{\rightleftarrows}} H_2(v=1, J=3)$$

of $k_{13}=2.2\times10^{-12}$ cm^3/s and $k_{31}=1.4\times10^{-11}$ cm^2/s are in good agreement with measurements using LIF spectroscopy in the VUV spectral region for H_2 (v, J) detection [6]. In a similar way, the vibrational energy transfer from $H_2(v=1)$ molecules can be studied. The diffusion of excited H_2 and HD out of the CARS beam strongly influences the time evolution of the CARS

signal. To estimate the influence of diffusion, an analytical expression for the solution of the kinetic equations coupled with transport processes is required. From such modelling calculations the rate constants for the vibrational energy exchange processes $H_2(v=1)+HD(v=0) \rightleftarrows H_2(v=0)+HD(v=1)$ $+\Delta E=469.4\,cm^{-1}$ of 1.9×10^{-13} cm^3/s in the exothermal and 1.4×10^{-14} cm^3/s in the endothermal direction are obtained.

The CARS detection system provides an ideal method for monitoring directly reactants and products in the $D+H_2(v=1)$ reaction. The reaction is followed in a discharge flow system, where the atoms and $H_2(v=1)$ molecules were generated by microwave discharges [7]. $HD(v=1)$ and $HD(v=0)$ molecules can be formed in adiabatic and non-adiabatic reaction pathways in this reaction. Information on the competition of reactive and inelastic channels can be obtained by monitoring the decrease of $H_2(v=1)$ in the presence of D atoms corrected for the energy transfer process described above. The experimental results obtained so far indicate about equal importance of inelastic and reactive channels as well as a predominance of the adiabatic over the non-adiabatic reactive pathways (see Fig. 3). The experiments show that when the H_2 molecule is excited to the first vibrational state, only about a third of the vibrational energy is used to overcome the potential energy barrier E_c [8, 9]. Thus the reaction of vibrationally excited hydrogen molecules still shows an energy barrier, whose height can be predicted both from classical and from quantum mechanical calculations of the course of reaction on the "ab initio" potential surface, in good agreement with experiments [7, 8]. As shown in the Arrhenius diagram of Fig. 3, only at low temperatures can significant differences between classical and quantum predictions of the reaction rate be expected. Such experiments are underway at the moment in our laboratory.

The results obtained from the study of the hydrogen exchange reaction on the efficiency of a selective vibrational excitation cannot be simply transferred to similar reactions. Thus investigations of the similarly thermoneutral reaction $^{37}Cl+H^{35}Cl(v=1)\rightarrow H^{37}Cl$ $(v=1,0)+{}^{35}Cl$ demonstrate the very effective use of the vibrational energy for overcoming the energy barrier [10]. The high efficiency with which the vibrational energy is used to overcome the energy barrier causes the chemical reaction, with increasing temperature, to proceed preferentially via the excited vibrational states. Thus, the temperature dependence of the reaction deviates significantly from that predicted by an Arrhenius equation [11]. The dynamics of the reaction has been simulated by classical, semiclassical, and quantum-mechanical calculations [10]. Particularly in very strongly endothermic reactions, vibrational excitation can be used efficiently for increasing the rate of the reaction. Thus, in the reaction [12] $Br + HCl(v) \rightarrow HBr(v=0) + Cl$ an increase in the reaction rate constant by more than 10 orders of magnitude can be obtained by vibrationally exciting the HCl molecule from $v=0$ to $v=2$. This dramatic increase in the rate constant can be used to separate chlorine isotopes (Fig. 4). ^{35}Cl atoms from HCl can be transformed in this way into $Br^{35}Cl$, which, because of its different chemical and physical properties, can be readily separated from the reaction mixture.

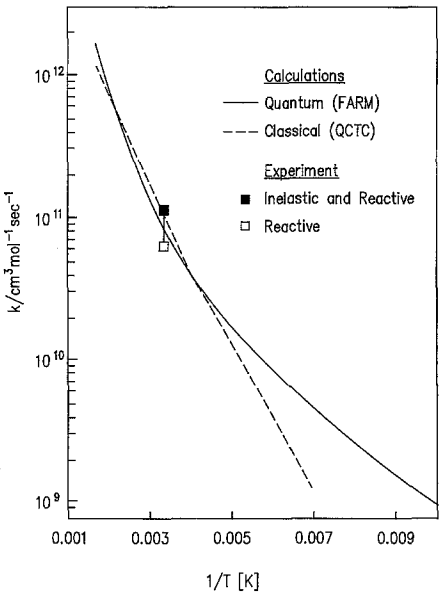

Fig. 3. Arrhenius diagram for the temperature dependence of the rate for the reaction $D + H_2\ (v=1) \rightarrow HD\ (v=1,0) + H$ [8]

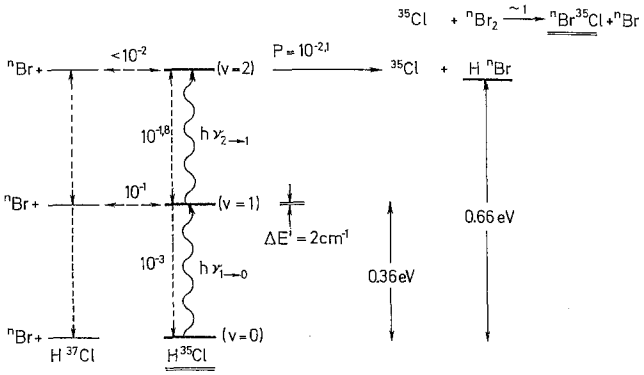

Fig. 4. Energy diagram for the reaction of Br atoms with isotope-selectively excited HCl molecules. P gives the probability for the transfer of vibrational energy between laser-excited $H^{35}Cl$ and $H^{37}Cl$ and for the course of a reaction in the various collision processes, respectively. The Br atoms react preferentially with $H^{35}Cl$ $(v=2)$. The resulting ^{35}Cl atoms further react with molecular bromine to give easily separated $Br^{35}Cl$. ΔE^i is the energy difference between $H^{35}Cl$ $(v=1)$ and $H^{37}Cl$ $(v=1)$

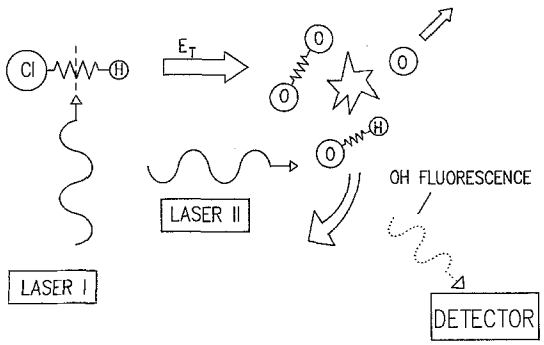

Fig. 5. Schematic for the investigation of reactions of translationally hot hydrogen atoms

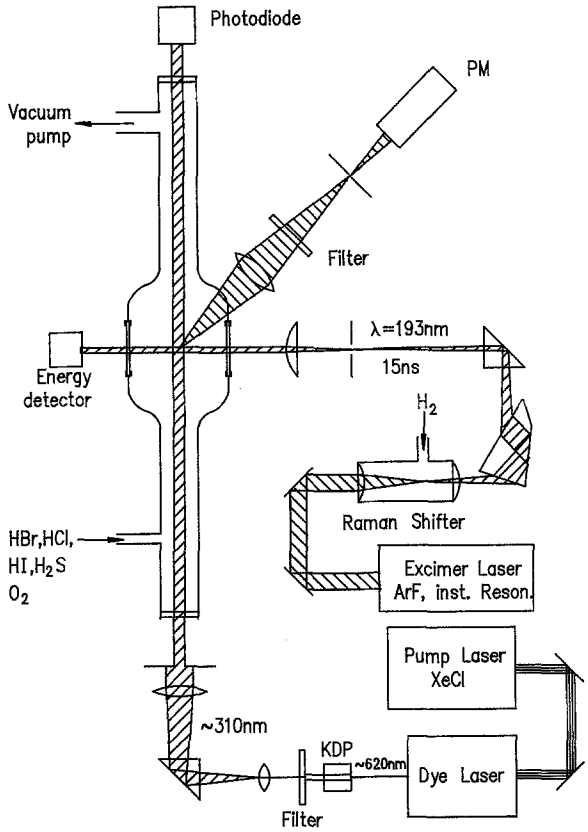

Fig. 6. Experimental arrangement for the study of reactions with translationally hot atoms and radicals by combination of excimer laser photolysis and LIF product detection

Despite the large number of elementary reactions taking place in the oxidation of hydrocarbons, important parameters of the combustion process are controlled by few elementary reactions. Sensitivity analysis shows that calculated flame velocities are relatively independent of reactions specifically for the oxidation of the fuel molecules. However, there is a strong influence on the calculated flame velocity from unspecific reactions, such as the reaction of hydrogen atoms with oxygen molecules $H + O_2 \rightarrow OH + O$ [13]. This endothermic reaction leads to the formation of two radicals and is therefore a very important chain-branching step. As shown in Fig. 5, the dynamics of such an elementary reaction with a high energy barrier can be studied in microscopic detail by combining translationally hot atom formation from laser photolysis with time-, state- and orientation-resolved product detection by laser-induced fluorescence spectroscopy. The apparatus is depicted in Fig. 6. Two laser beams are directed perpendicular through a flow reactor equipped with long side arms to reduce the scattered light from the dye laser analysis pulse. Fluorescence light is detected as a function of the dye laser wavelength through emission optics and a filter by a photomultiplier. The experiments show [14] that the major part of the relative translational energy of the reactants is converted into rotational energy of the product OH, in agreement with the results of quasi-classical trajectory calculations [15].

The observed rotational energy distributions give interesting microscopic details on the molecular dynamics of these elementary steps. Spin-orbit and orbital-rotation interactions in the OH radical cause fine structure splittings for each rotational level. Each of these fine structure levels can be probed by different rotational sub-bands. The two OH spin states $^2\Pi_{1/2}$ and $^2\Pi_{3/2}$ are, within experimental error, equally populated. The Λ-doublet fine structure states show a clear preference for the lower energy $\Pi^+(A')$ component. The experimental results indicate that break-up of the reaction complex generates forces in a plane containing the bond to be broken. The OH radical rotates in that plane and J_{OH} is perpendicular to it and to the broken bond. This picture is consistent with a preferential planar exit channel in these reactions. This could also be directly demonstrated by using polarized photolysis and analysis laser beams [16]. The physical difference between the two Λ-doublet components $\Pi^+(A')$ and $\Pi^-(A'')$ arises from interaction of the electronic spin-orbit momentum with the rotation of the molecule. For fast rotation of the OH radical, the unpaired electron in the p orbital of the oxygen is no longer able to follow the movement of the atomic nuclei. If the p orbital lies in the OH rotational plane, the electron distribution on the oxygen atom changes, becoming increasingly spherical. In contrast, for a $\Pi^-(A'')$ configuration, the oxygen atom moves in the nodal plane of the p orbital and thus continues to "see" a dumb-bell-shaped electron environment, even for fast rotation. This leads to a splitting of the energies of the $\Pi^+(A')$ and $\Pi^-(A'')$ configurations, which selectively increases with increasing rotational energy. At 1.8 eV collision energy, about three OH radicals were found in the $\Pi^+(A')$ state for each OH radical in the

$\Pi^-(A'')$ state. This shows that the unpaired electron formed after bond cleavage of O_2 stays in an orbital in the rotational plane of the OH radical. During the reaction, most of the HO_2 complexes do not rotate out of the initial plane (see Fig. 7), which can be understood on kinematic grounds [17]. Experimentally, a total reaction cross-section of 0.42 ± 0.2 Å^2 at $E = 2.6$ eV is found [14]. The theoretical reactive cross-section obtained under these conditions by quasi-classical trajectory calculations [15, 18] on the Melius and Blint [19] surface is 0.38 Å^2. These numbers cannot be compared directly, because the multiplicity of the $^2A''$ surface and the influence of the first electronic excited state of HO_2 are not taken into account. The observed discrepancies may be attributed to a reduction of the calculated reaction cross-section due to a "rigid" character and a barrier of 8 kJ mol^{-1} in the Melius-Blint surface for dissociation of the HO_2 in the reaction $HO_2 + M \rightarrow H + O_2 + M$ [20]. Later calculations [21, 22] reduce this barrier. Also for the reaction (-1) $O + OH \rightarrow O_2 + H$ the Melius-Blint surface apparently overestimates the long-range O–OH attraction, while the Quack-Troe interpolation scheme [20] leads to better agreement with the experimental values at low temperature if the two lowest electronic states of the HO_2 radical are taken into account. Calculated rate coefficients obtained by using this theoretical cross sections from the surface [18] are in agreement with shock tube measurements for k_1 by Schott [23]. However, recent shock tube experiments [24, 25] using time-resolved atomic resonance line absorption give higher values for k_1, in agreement with the reactive cross-sections obtained in state-selective experiments. This example shows that even for a very simple chemical elementary step in combustion more work has to be done on the potential energy surface to obtain satisfactory agreement between the results from quantum chemistry and state-selective and thermal experiments using laser stimulation and detection.

2. Chemical Synthesis with Lasers

It would seem obvious to use the methods described for the selective control of chemical reactions by vibrational excitation for making new products or improving synthetic procedures. Under the typical conditions of industrial chemical processes (high pressures, reactions in the liquid phase, large molecules), a selected molecular state cannot, in most cases, be held stable until the reaction stage. The exchange of energy between the degrees of freedom within a molecule and between various molecules usually occurs on the 10^{-14} to 10^{-10} s time-scale and is therefore generally considerably faster than the reaction itself. On the other hand, nonthermal isomer and isotope distributions as

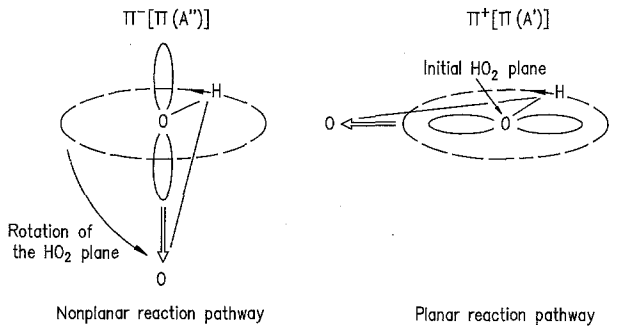

Fig. 7. Vector properties of the $H + O_2 \rightarrow OH\ (N, v, f)$ reaction

well as nonthermal radical concentrations from laser-induced dissociation and isomerization processes can readily be maintained under industrial chemical conditions and used for the production of new, particularly pure products, or products obtained with low energy consumption. Here, the use of the laser offers a number of advantages over conventional light sources: extension of the available wavelength range; the selective excitation of just one kind of molecule, e.g. for isotope separation or ultra-purification because of the narrow spectral bandwidth of the laser light; spatially and temporally controllable, homogeneous excitation of the reaction volume because of the possibilities of pulsed operation and strong collimation; the possibility multiphoton excitation because of the high spectral density. Hg or Xe lamps are mostly used as light sources for industrial photochemistry. Laser photons have to compete both in investment and operational cost as well as in maintenance expenditure, long term power, and lifetime. For economic application of lasers in this area, the effective cost of the photons produced must lie considerably below that for the desired product. One should remember that, generally, the product price is determined only to a small extent by the photochemical step involved in the production and that techniques employing lasers have to compete not only with a conventional photochemical processes, but also with other methods of synthesis. Ideally, the use of lasers should result in several improvements simultaneously, such as cheaper starting materials, fewer or more valuable by-products, and fewer or cheaper process steps. In particular, the production of cheap mass-produced chemicals using lasers is only worthwhile if very high quantum yields (number of product molecules produced per photon generated) can be achieved in radical chain reactions.

Vinyl chloride (VC), the monomer of PVC, is produced industrially mainly by thermal cleavage of HCl from 1,2-dichloroethane (DCE) by a chain reaction. With a world-wide production volume of over 25 $\times 10^6$ tonnes per annum, VC is one of the leading products of the chemical industry as far as quantity is

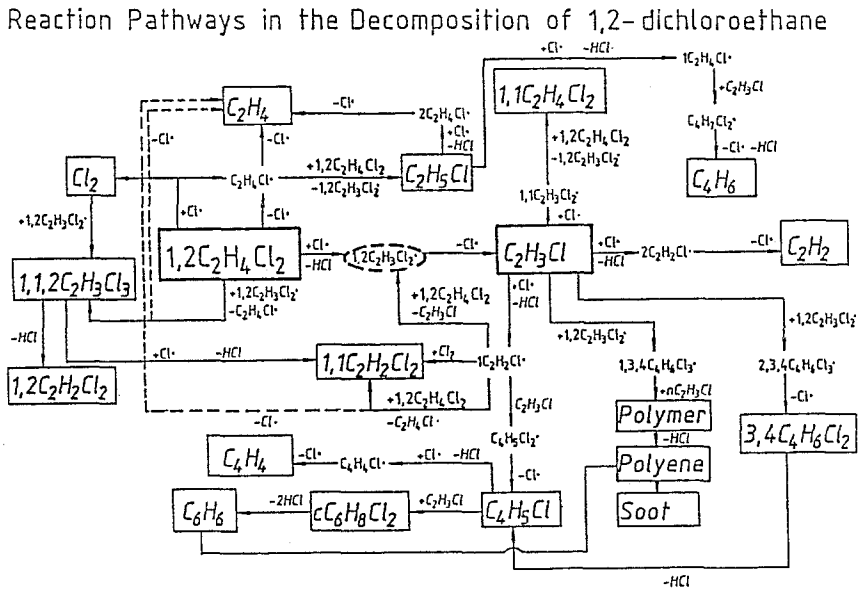

Fig. 8. Reaction paths for the cleavage of hydrogen chloride from dichloroethane, ($1,2\text{-}C_2H_4Cl_2$), in a laser-induced chain reaction

concerned. The advantage of photolytic over thermal initiation of the chain reaction is that the unimolecular process $C_2H_3Cl_2 \rightarrow C_2H_3Cl + Cl$ is rate determining with a low energy barrier. This leads to a low activation energy for the total reaction and hence low reactor temperatures, higher conversions, and fewer by-products [26]. The use of laser radiation to initiate the chain reaction also permits detailed investigations of the reaction kinetics. Radicals may thereby be produced in a wide concentration range and the reactions followed as a function of time. The experimental data can be compared with those obtained from a kinetic model, which for a given temperature and pressure simulates the whole course of reaction (Fig. 8) by using a system of coupled differential equations for the elementary chemical steps. From a comparison of the experimental data with the predictions of the model, missing rate constants of selected elementary steps can be determined [27]. The data so obtained on the pressure and temperature dependence of the laser-induced VC formation can then be used to predict the DCE–VC conversion efficiency for industrially realistic conditions. The calculations show a clear increase in the conversion ratio after laser photocatalysis. This provides a method of using UV-laser radiation to improve a large-scale industrial process. A pilot plant presently under construction is shown schematically in Fig. 9. The thermal cleavage of DCE takes place in a tubular reactor. After heating the DCE, a segment of the reactor can be irradiated with a powerful excimer laser. The laser is tuned to a wavelength at which the absorption in the medium is as small as possible. Due to the highly parallel nature of the laser beam, a very large volume can be irradiated and a steady, small concentration of active chlorine atoms, and hence long

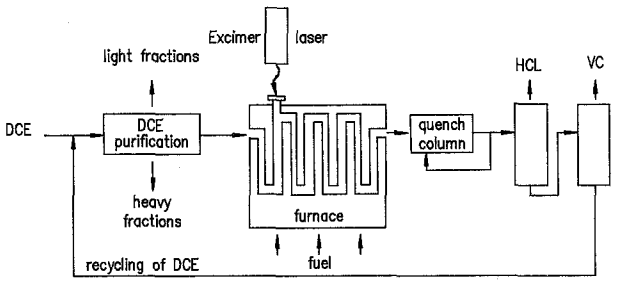

Fig. 9. Pilot plant for the production of vinyl chloride using an excimer laser

chains, are produced. At the same time, irradiation of the wall and hence the initiation of heterogeneous processes is, to a large extent, avoided. With laser radiation, faster conversion at lower temperatures can be achieved compared with the previous process. Thus higher total conversions with simultaneously reduced formation of by-products are possible.

Another way to multiply the effect of laser photons in chemical synthesis is the production of catalysts with laser radiation. By laser pyrolysis of gas mixtures, catalytically active solids of variable composition can be produced (Fig. 10). On complete mixing of the gaseous starting materials and rapid heating in the laser beam, very small solid particles with homogeneous structure and large surface area are obtained, whose composition can be varied over a large range. By optimizing the composition of the laser-synthesized Fe/Si/C catalysts, higher selectivity and preferential formation of the valuable light olefins (C_2–C_4) can be achieved [28]. With the arrangement shown in Fig. 10 fine chrome oxide powders can be produced for the selective catalytic dehydrogenation of saturated hy-

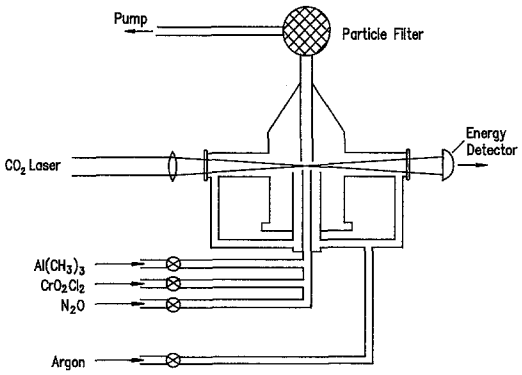

Fig. 10. Synthesis of chromiumoxide catalysts by CO_2 laser pyrolysis of gaseous starting materials. By varying the partial pressures of the component and the laser intensities, catalysts with varying properties can be produced [28, 29]

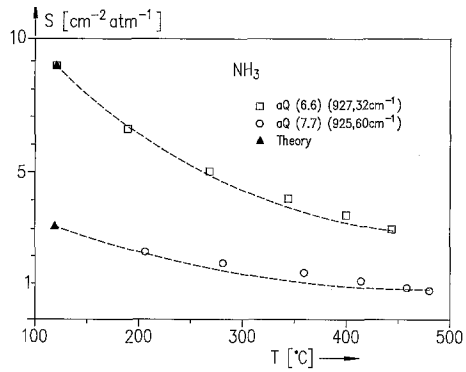

Fig. 11. Temperature dependence of absolute absorption cross sections of NH_3 lines measured with a tunable IR diode laser

drocarbons [29]. Metal carbonyl catalysts can be UV-photoactivated instead of thermally activated. Active centres are formed by cleavage of one or more CO ligands, often resulting in catalytic activity, even at room temperature. Besides polymerization, the isomerization and hydration of alkanes with $Fe(Cl)_5$ catalysts [30, 31] and the silylation of alkanes and aldehyde with $Co_4(CO)_{12}$ catalysts upon irradiation with a XeF laser or a frequency-doubled Nd YAG laser, have been investigated. For the isomerization of 1-pentene, quantum yields of 10^3 and "turn-over" rates (quantum yield per average lifetime of the catalysts) of $4 \times 10^3\ s^{-1}$ at 50% conversion of 1-pentene can be achieved. Broad-band light sources, such as flash lamps, lead more readily to direct photolysis and to undesired by-products.

3. Laser Spectroscopy of Industrial Chemical Processes

3.1. Application of IR *Laser Spectroscopy to In Situ Monitoring of* NH_3 *in Power Plants*

Inhibition and sensitization of chemical processes by nitric oxide are well-known phenomena. Recently, the role of the nitrogen oxides in the formation of acid rain, photochemical smog and the possible depletion of the stratospheric ozone layer has stimulated interest in chemical reactions which can selectively remove nitrogen oxides. An interesting elementary chemical reaction in this respect is the reaction of nitric oxide with the NH_2 radical. First direct studies of the rate and products of this reaction showed a very fast complex addition rearrangement sequence which forms nitrogen molecules and highly vibrational excited water molecules in the single step [32]: $NH_2 + NO \rightarrow N_2 + H_2O^*$. Using time-resolved infrared emission combined with laser photolysis, direct measurements of the distribution of reaction energy in the water molecule formed in this reaction can be carried out [33]. An enlarged volume for the production of NH_2 radicals by photolysis of NH_3 is created by multi-reflection of an ArF exciplex laser beam combined with a Welsh-mirror light gathering system for the effective collection of infrared fluorescence from excited H_2O molecules. The spectrally resolved infrared emission can be approximately simulated with a vibrational temperature for the H_2O molecules formed of 10^4 K. Significantly lower vibrational temperatures are found in the nitrogen molecules by CARS spectroscopy [33]. The reaction is very selective in channelling the available reaction energy preferably in the stretching vibrations of one reaction product. Therefore, many simultaneous and competing pathways have to be considered in a simulation of the selective reduction of NO by NH_3 in the presence of various amounts of O_2 [34, 35]. Such model calculations can now be applied to realistic situations. Under these conditions one observes a very rapid reduction of NO at the optimum temperature. The model also indicates that rapid mixing of NH_3 with flue gases is essential to obtain optimal reduction results. This can be achieved by using steam or other media for producing a high momentum of the injected material. The main practical problem remaining is the control of the ammonia injection level and location such that breakthrough of NH_3 is avoided under varying combustion conditions. This problem can be attacked by using laser methods for in situ monitoring of NH_3. Figure 11 shows absolute absorption cross sections for NH_3 absorption lines at higher temperatures obtained with a tunable diode laser system. Using $^{13}CO_2$ in an infrared waveguide CO_2-laser, one observes coincidences between NH_3 and $^{13}CO_2$-laser lines in spectral regions where other components of the flue gas (H_2O, $^{12}CO_2$, SO_2, hydrocarbons) do not absorb significantly. The $^{13}CO_2$

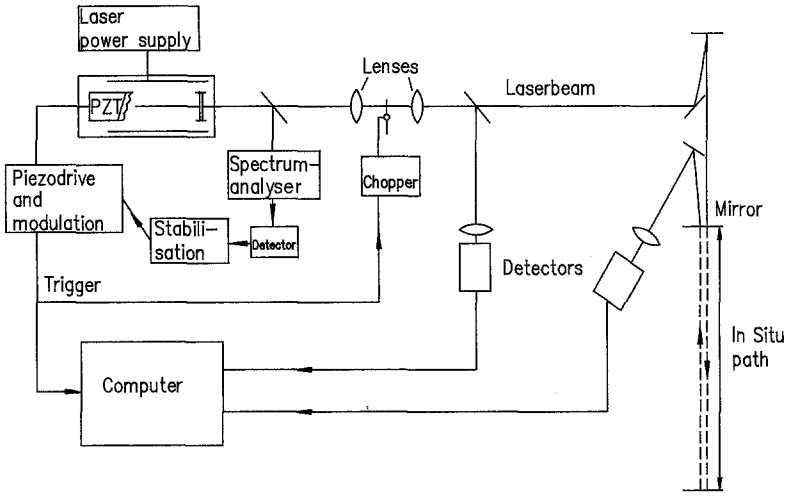

Fig. 12. In situ detection of NH_3 in power plants using differential absorption

laser lines have a bandwidth of less than 0.01 cm^{-1} while the distance to the line centre of the NH_3 line can be as little as 0.02 cm^{-1} where the NH_3 line width is 0.08 cm^{-1}. By choosing a suitable reference line and a multipath absorption arrangement, one can achieve a detection sensitivity of less than 1 vppm for in situ measurements of NH_3 concentrations at higher temperatures by differential absorption [35] with kHz repetition rates (see Fig. 12).

3.2. Non-Intrusive Temperature Measurements in Counter-Flow Diffusion Flames with CARS *Spectroscopy*

Industrial chemical processes are characterized by a very complex interaction of elementary chemical reactions and various transport processes. Measurements of temperature by thermocouples, and of concentrations of chemical reacting species by probe sampling, can greatly disturb this complicated balance and give results greatly in error. The development of non-intrusive laser methods for monitoring industrial processes opens up new ways to obtain unperturbed information on the temperature and species concentrations which can be compared with detailed mathematical modelling.

Laminar counter-flow diffusion flames constitute an important basis for the simulation of turbulent combustion processes [36]. Having a library of precalculated "flamelets" at different strain rates and fuel/oxidizer mixture compositions, the numerical treatment of turbulent flame structures with a "flamelet model" [37] is reduced to a problem that can be solved within a reasonable amount of time on existing computers. Therefore, there is renewed interest in the study of diffusion flames under a variety of different burning conditions to test and refine the validity of chemistry and transport properties in modelling these flame structures. Among the different types of counter-flow diffusion flames the configuration where the flame is established in the forward stagnation region of a cylindrical porous burner offers some inherent advantages [38]. A schematic drawing of the burner configuration is shown in Fig. 13. A simple nearly 1-dimensional interaction of laminar flow and chemical reaction can be realized in this way. Two beams emitted by a Nd:YAG laser (Quanta Ray DCR1A) at 532 nm were used to pump a broad-band dye laser which delivered about 10 mJ at the Stokes shifted wavelength. The pump beams were achieved by sequentially doubling the fundamental and residual 1.06 μm output from the first frequency doubler. The secondary green beam was used to transversely pump the Stokes dye oscillator. A Brewster plate polarizer ensured an output beam 90% vertically polarized. The dye laser and part of the 532 nm pump beam (30 mJ) were collinearly combined in a USED–CARS phase matching geometry [39]. The CARS signal emerging from the measurement point (actually a cylinder approximately 60 μm in diameter and 1 mm long) was filtered off the residual pump and Stokes beams components and dispersed in a 1.3 m monochromator (McPherson Mod. 209) equipped with a 2400 l/mm holographic grating. The linear dispersion in the plane of the intensified diode array camera (Sl, Mod. IRY, 512 pixels) mounted behind a magnifying lens was measured to be 0.14 cm^{-1} per diode pixel. Throughout the experiments possible non-resonant CARS contributions complicating data evaluation [40] were suppressed by polarization techniques [41]. Averaged spectra (typically 300 laser shots) were stored in a laboratory computer and transferred to a larger computer (IBM 3090–180) for further analysis. Temperatures were deduced from computer-generated least-squares fitting spectral shapes of nitrogen vibrational-rotational Q-branch CARS spectra to measured spec-

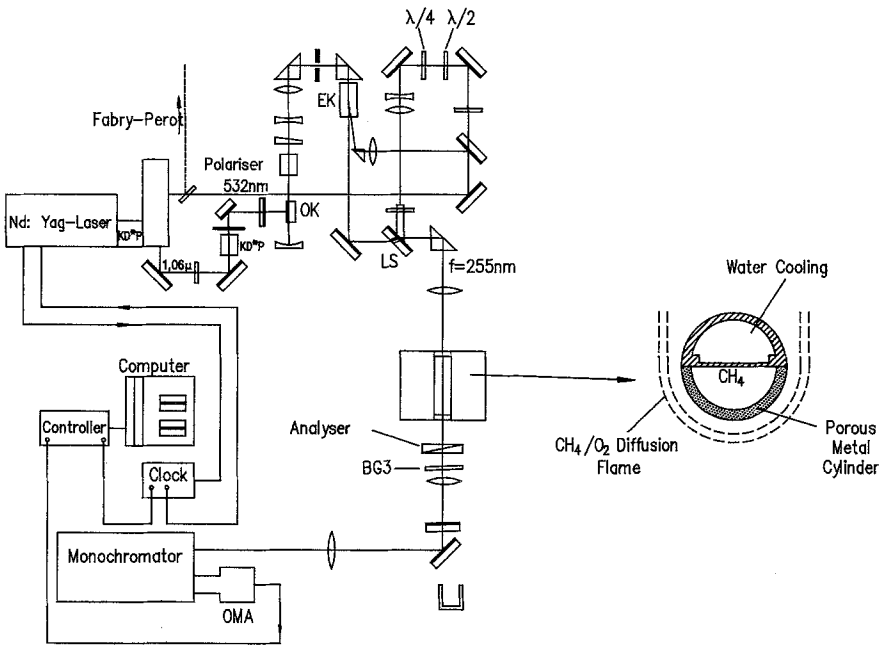

Fig. 13. Experimental arrangement for measuring temperature and concentration profiles in a counter-flow diffusion flame with broad-band USED–CARS

tra with temperature as a variable parameter. To get precise information on temperature from CARS spectra, a simulation program has to take into account collisional narrowing effects [42]. Another influence resulted from cross coherence effects induced by using a multimode laser as a light source in generating CARS spectra. This phenomenon accounts for partial coherences in the CARS signals [43, 44]. Cross coherence effects are mainly induced when correlated laser fields are used in generating CARS signals leading to convolution procedures different from the classical descriptions given by Yuratich [45]. Following a procedure of Koszykowsky et al. [46], the temperature-dependent part of the complex G-matrix was diagonalized. If the off-diagonal elements in the G-matrix – which describe the relaxation rates between states of different energy in the colliding molecule and therefore are responsible for collisional narrowing – were ignored, the previously used isolated line model results. In the current version of the fitting program, routines were included which use the closed form solution of Greenhalgh and Hall [43]. For the fitting routine, the procedure commonly used was replaced by orthogonal "Householder" transformations [47]. To reflect the real measurement situation, the distortion of the spectrum by the detector and spectrograph instrument functions as well as the pump laser linewidth had to be included in the simulation program by appropriate convolutions. Best result have been obtained by a priori fitting of these parameters to a CARS spectrum taken at room temperatures. Figure 14 shows a nitrogen Q-branch CARS spectrum taken in a counter-flow diffusion flame together with the spectrum simulation. In Fig. 15 temperature profiles measured by CARS in counter-flow diffusion flames with velocity gradients $a=2v/r=250\,s^{-1}$ and $350\,s^{-1}$ (v=free stream air velocity, r=radius of the porous burner) are shown together with the numerical results [48]. The measured locations of the temperature maxima agree quite well with those of the calculated ones. The general shapes and widths of the profiles as measured with CARS are very similar to those of the calculated profiles while previous thermocouple measurements [38] show significant discrepancies. The

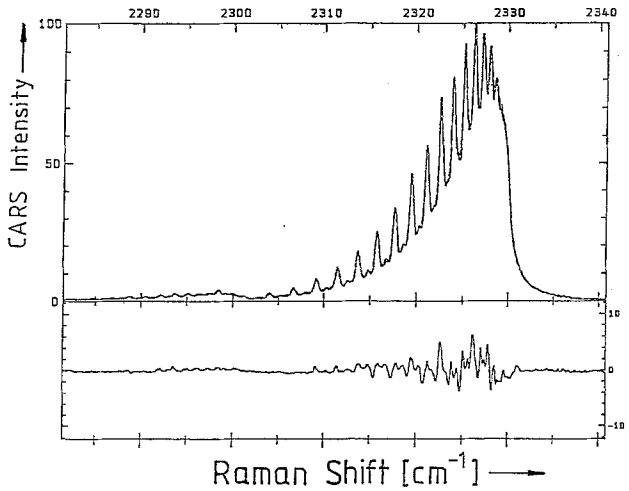

Fig. 14. Nitrogen Q-branch CARS spectrum taken at 2.6 mm from the burner head in the $a=200\,s^{-1}$ counter-flow diffusion flame. The best fit spectrum, characterized by a temperature of 1870 K, is shown as a dashed line together with the residuals of both signatures (lower trace in the figure)

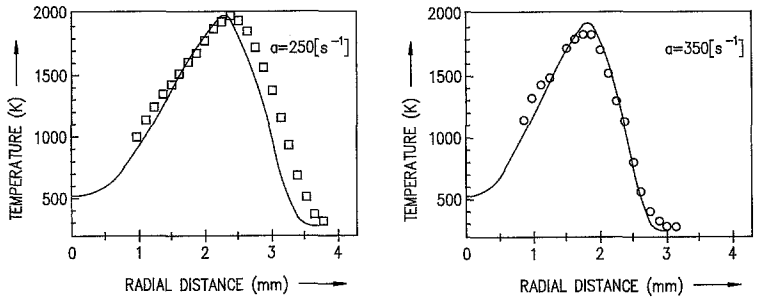

Fig. 15. Temperature profiles calculated (lines) and measured by CARS (□, ○) in CH_4/air counter-flow diffusion flames with different strain rates ($a=2v/r$)

computed peak temperatures in all cases are a little higher than those measured by CARS. This may be partly attributable to the fact that radiative losses are not included in the modelling calculations. Heat flux to the cylinder may be of increasing importance for higher velocity gradients. Similar results are obtained for concentration profiles.

3.3. 2-D Species Concentration Imaging in Turbulent Reactors

The application of planar laser-induced fluorescence (LIF) [49] gives access to multidimensional species concentration and temperature and velocity information in reacting flows [49]. As shown in Fig. 16, the intensity of the fluorescence signal can be expressed by the spectroscopic parameters, the ground state population and the electronic quenching rate (Q). Since at atmospheric and higher pressures, fluorescence lifetimes (equivalent to $1/Q$) for many key species in combustion are of the order of nanoseconds or less, an ultra-short-pulse laser coupled with fast detection and data acquisition/processing is required for direct measurements. The hydroxyl radical is an important intermediate in all flames containing hydrogen and oxygen and can serve to indicate the progress of combustion. In laminar atmospheric methane/air flames, for example, concentrations of up to several thousand ppm are generally observed. The laser wavelengths required for excitation are convenient and the fluorescence from the Meinel bands can be used for sensitive detection. Time-resolved measurements were made with a home-built picosecond dye laser (Fig. 17), using an excimer pump laser (308 nm, EMG MSC 103 Lambda Physik). The starting pulse length of 8 ns was shortened first in a quenched transient dye laser (QDTL), which operates by suppressing resonator

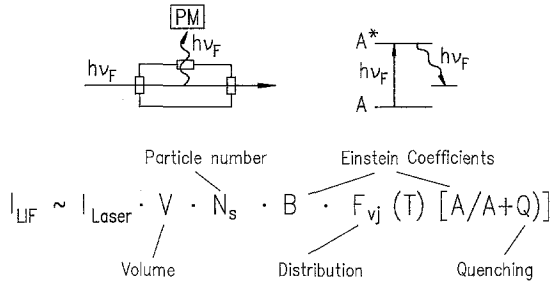

Fig. 16. Principles of laser-induced fluorescence spectroscopy

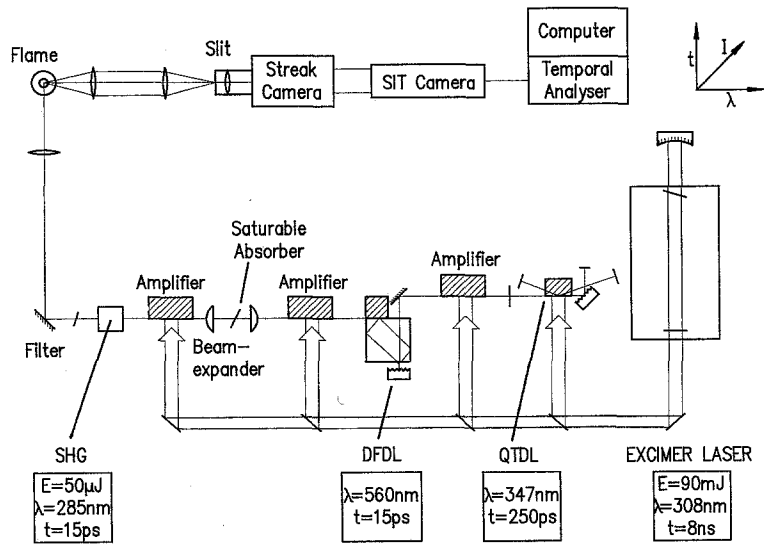

Fig. 17. Experimental set-up for fluorescence lifetime measurements in atmospheric pressure flames. DFDL (distributed feedback dye laser) QTDL (quench transient dye laser) SHG (second harmonic generation)

transients in a double resonator system [50]. After amplification, these pulses were used to pump the oscillator of the second stage, the distributed feedback laser (DFDL) [51]. In the DFDL, feedback is provided by Bragg scattering from spatially periodic perturbations of the optical gain and pulse shortening achieved by spatial separation of the first resonator peak from the following peaks [52]. For OH(A–X) excitation, rhodamine B was used in the DFDL cuvette. The second harmonic of the laser frequency was generated by passing the beam through an 8 mm long crystal of β-BaB_2O_4. A UV pulse of 15 μJ energy was used with a repetition rate of 1 Hz. The laser beam was directed into an atmospheric pressure, water-cooled (thermostat 50 °C) burner of the flat-flame type. Premixed flows of methane/air were supplied to the burner using Tylan mass flow controllers. Integrated fluorescence from the OH radicals was observed at right angles to the focussed laser beam. Fluorescence light was focussed onto the 100 μm × 15 mm slit of a streak camera (C1587 Hamamatsu, S-20 photocathode), a streak time of 10 ns per 15 mm was set and the data were interpreted by a temporal analyser (Hamamatsu C2200).

For most measurements, the $Q_1 5$ line at 308.52 nm was excited. Measurements of the OH(A–X) lifetime were made at different heights above the burner surface, i.e. from 0.5 to 20 mm, also with a constant height of 20 mm but varying ϕ from 0.77 to 1.43. Within experimental error, no change in lifetime could be discerned in either series of measurements (see Fig. 18). The experimental result, that the collisional quenching rate is constant throughout an atmospheric pressure of flame although for different mixing ratios, allows the determination of absolute number densities in such flames, as shown in Fig. 19. By combining an integrated absorption measurement with spatially resolved LIF [54]. Figure 19b and c shows the OH radical concentration in an unperturbed and perturbed Bunsen burner flame.

Various methods of imaging flame fronts in combustion and flow processes using dopants have been described. Some of these are based on the seeding of particles into the flow to be investigated. For example, $TiCl_4$ added to the combustion chamber reacts with water formed in the flame front to form TiO_2 particles, which can serve as centres for Mie scattering and can be used for 2-D visualization. However, such methods involve complex data processing and are not always applicable (e.g. due to particle lag). These limitations can be largely overcome by seeding with fluorescent dopants. Experiments using acetaldehyde as dopant will be described here [56]. Detailed investigations on LIF of acetaldehyde in supersonic jets [57] have provided information on the rovibronic levels of the S_1

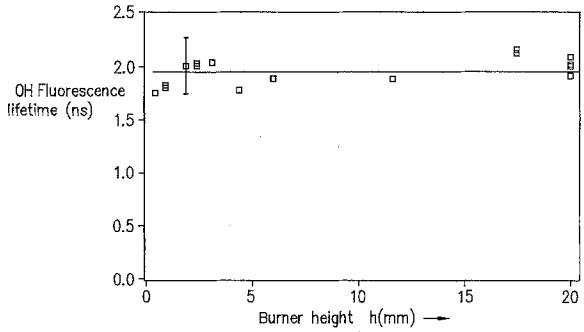

Fig. 18. Lifetime measurements of OH excited at 308.52 nm ($Q_1 5$ line) at various heights in a laminar premixed methane/air flame at atmospheric pressure

state below the photodissociation threshold together with lifetimes for many of these levels, and a more reliable value for the origin of the S_1 state. The conclusion of studies was that the dominant relaxation process from lower vibrational levels of the S_1 is irreversible internal conversion to S_0. Studies of the dependence of acetaldehyde fluorescence on added gas pressures up to 25 bar establish that this molecule is a suitable tracer to show up the flame front in an internal combustion engine using the set-up shown in Fig. 20a. The combustion engine, which was supplied by Daimler-Benz, was operated as a compression expansion machine with a square cross section cylinder to allow easy access for line-of-sight measurements. The XeCl excimer laser light sheet (308 nm) entered the combustion chamber through a quartz window on the cylinder head. The LIF signal from the acetaldehyde in the detection region (35 × 35 mm) was collected by the imaging optics of the image-intensified CCD camera. Stray light was supressed by inserting a interference filter between the imaging optics and the chamber and attaching a dielectric mirror to the top of the piston to reflect the laser beam out of the combustion chamber. Fluorescence images were digitized and processed by a frame grabber (MATROX MUP-AT) and connected to a personal computer (Zenith Z386). Images were then taken at different times after ignition (Fig. 20b), using a detection region of approximately 35 × 35 mm. The bright parts of the image are those where the acetaldehyde/propane/air mixture is still present, in contrast to the dark parts of the image where the fuel has been burnt. The boundary between the burnt and unburnt zones can easily be recognized. Only a small zone with an intermediate concentration of the gas mixture can be seen between the unburnt and burnt regions. The small zone of intermediate fluorescence intensity could not primarily represent a temperature gradient between the flame front and the region of unburnt fuel, since no significant fall in acetaldehyde fluorescence yield with temperature could be observed.

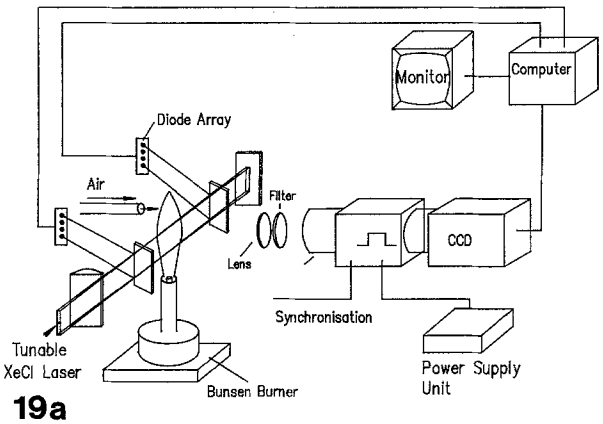

19a

Fig. 19a–c. Determination of 2-*D* instantaneous OH concentrations in flames using tunable excimer lasers. (a) Experimental set-up. (b) OH distribution in an unperturbed Bunsen burner flame. (c) Perturbed flame

Fig. 20 (a) Experimental set-up for imaging experiments in an internal combustion engine. (b) Imaging of the flame front in an internal combustion engine using acetaldehyde for imaging the flame front in the engine after ignition (burnt parts are the dark regions)

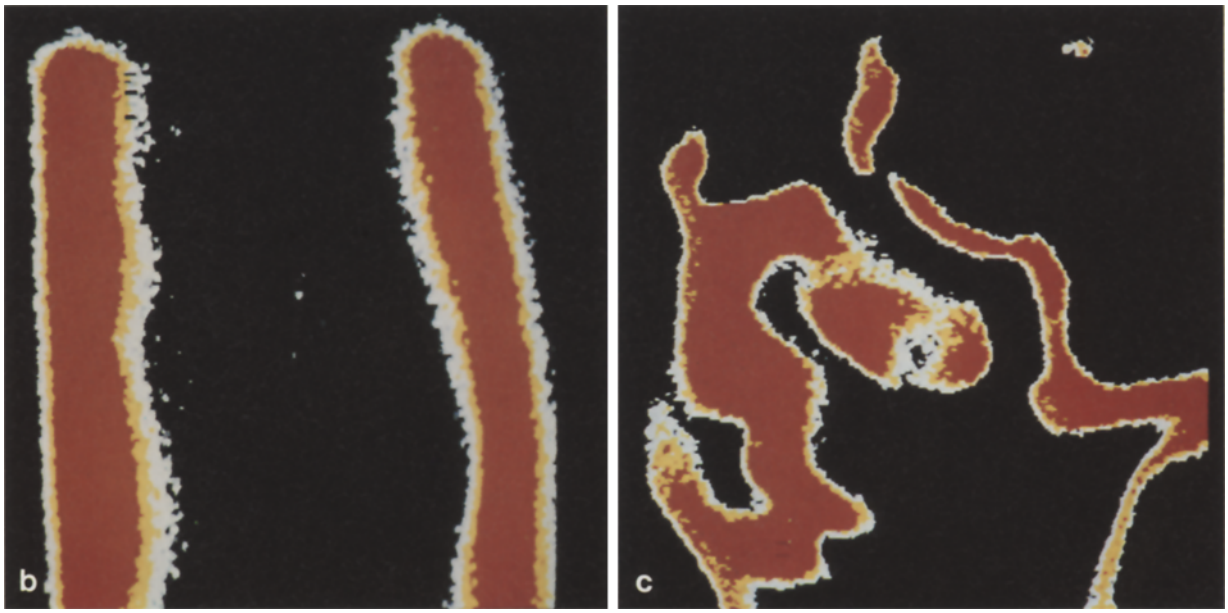

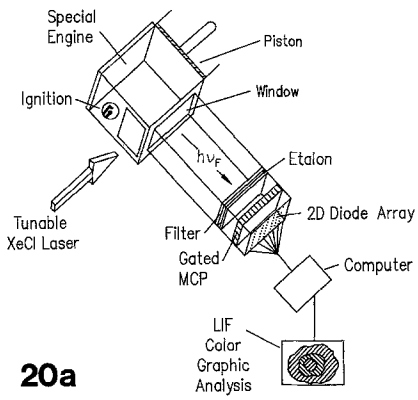

20a

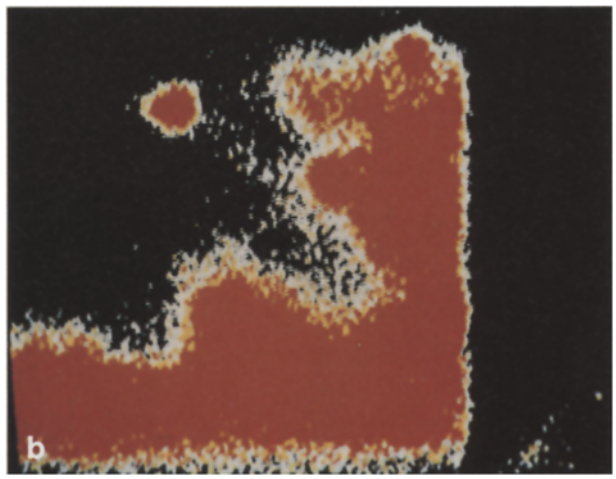

4. Lasers in Genetic Engineering

Many of the spectroscopic techniques described above can also be applied in biochemistry and biology. While biological applications of nonlinear techniques such as CARS or REMPI are still in their infancy, other techniques have contributed valuable information to our knowledge of life processes. For example, practically all information on the primary processes of vision and photosynthesis, i.e. the fast processes where the

physical stimulus is transferred into chemical reactions, stems from (sub-)picosecond absorption spectroscopy [58, 59]. Laser-induced fluorescence, due to its high sensitivity, is particularly suited to the study of biological molecules which are available only in small amounts or which are poorly soluble in water, the natural solvent of many biological molecules. A very attractive application of LIF is the study of protein-DNA binding, which is governed by electrostatic interaction of the positively charged amino-acids lysine and arginine with the negatively charged DNA, and by stacking interactions of the aromatic amino-acids tyrosine and tryptophane with the heterocyclic bases of DNA. The aromatic amino-acids reveal intense fluorescence in the ultraviolet. When they bind to DNA, they transfer their fluorescence energy to the latter, which is essentially dark [60]. This fluorescence can therefore be used as a probe of the binding process. LIF experiments have been used to elucidate the binding kinetics of peptides such as lysine-tyrosine-lysine to DNA. These peptides first bind unspecifically via electrostatic bonds and in a second step specifically (i.e. recognizing topological features of the DNA) via stacking [61]. Such a stacking interaction also seems to be responsible for the stabilization of a simple bacterial virus, the phage Pf1, and for an unusually large base-to-base distance in a rare structural form of DNA (inverted DNA) [62].

LIF experiments have also been used to study the electrostatic part of protein-DNA interaction. While lysine forms pure electrostatic bonds [63], LIF has revealed that arginine interacts via a mixture of electrostatic and non-electrostatic bonds [64]. This difference may explain why, in the life of a biological cell, arginine-rich proteins are occasionally replaced by lysine-rich proteins.

Studies of the wavelength dependence of laser interactions with the surface of human red blood cells have shown that UV photons interact much more effectively with biological cells than visible or IR light [65]. This finding has led to the extension of laser microbeam techniques [66] to the ultraviolet.

A UV laser microbeam can be realized by an excimer-laser-pumped dye laser, the pulses of which are coupled into a microscope and focussed to the diffraction limit. At the focal point, energy densities of 10^{10}–10^{12} W/cm^2 can be obtained. These energies are sufficient to manipulate biological objects with spatial accuracy of the wavelength of the light used, and even below that, if nonlinear effects can be exploited. Spatial accuracy is not only obtained in the object plane but also along the optical axis. Because energy densities sufficient for manipulation of biological material are obtained only a few hundred nanometres above and below the focal point, one can manipulate subcellular structures in a cell without opening it. This UV laser microbeam can thus be used for the treatment of biological cells and subcellular structures. For example, individual cells can be fused under total microscopic control [67, 68], genetic material can be introduced into plant cells [69] and chromosomes can be dissected into small portions [70].

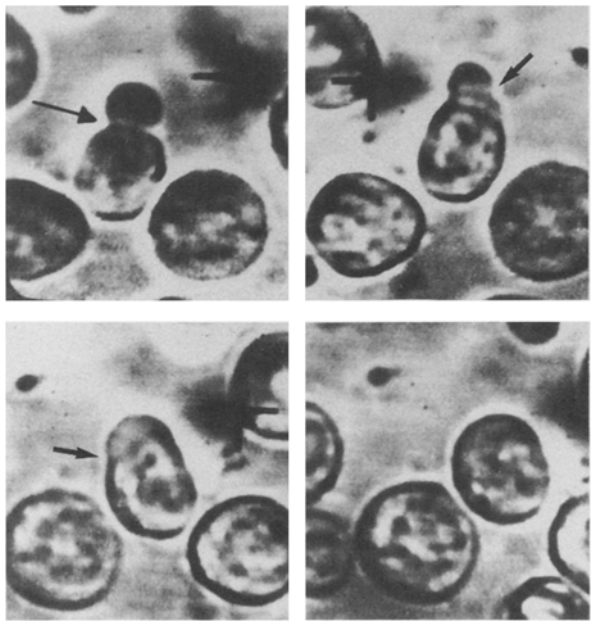

Fig. 21. Fusion of a mouse *B*-lymphocyte with a mouse myeloma cell

Figure 21 gives a series of photographs of a cell fusion process, taken from a microscope at a magnification of 1000. The small cell is a *B*-lymphocyte, a cell from the immune system of a mouse, capable of producing antibodies. In vitro *B* lymphocytes die after 3–4 generations, i.e. they cannot be held in culture. The large cell is a long-lived myeloma (blood cancer) cell. Both cells are induced to fuse by a few UV pulses focussed on the contact area. The major advantages of this laser-induced cell fusion, as compared with conventional cell fusion techniques, are the total microscopic control and the fact, that the process occurs under physiological conditions. Therefore, even fragile cells have a chance of surviving the fusion process. By combining laser-induced fusion with coupling of the two fusion partners via an antigen-avidin-biotin bridge [72], one can preselect those *B*-lymphocytes which have the potential to produce antibodies against a given antigen. Only those *B*-lymphocytes are fused with myeloma cells to give hydridoma, the long-lived fusion products with the potential to produce antibodies in vitro. Based on this technique, a method is being developed which avoids the lengthy search for the hybridoma specific for the "wanted" antibody. If

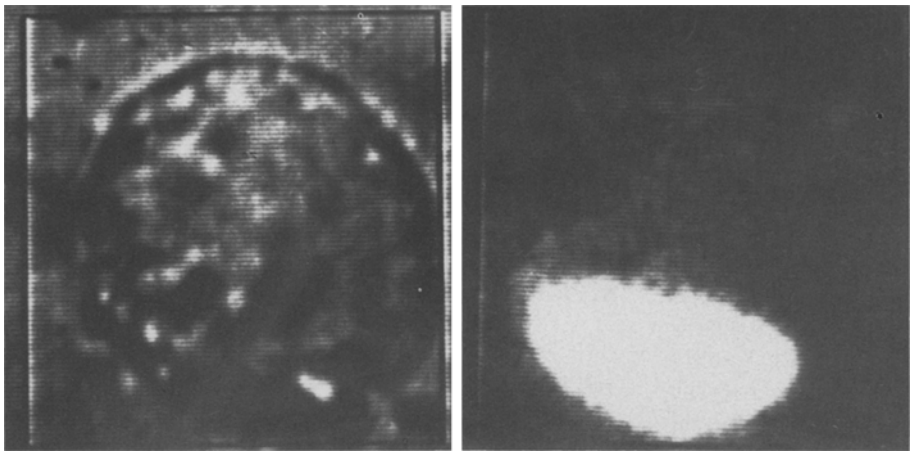

a b

Fig. 22a, b. Injection of fluorescently labelled DNA into a rape cell using an UV laser microbeam

some remaining cell-biological problems can be solved, this may become the basis for a fast, specific production of monoclonal antibodies for cancer therapy. Such a fast method is required since cancer cells change their susceptibility to a special antibody within weeks, while present methods for the production of antibodies take months to years.

Figure 22a shows a plant cell in which foreign DNA has been injected by use of the UV laser microbeam. A self healing hole of 0.5 to 1 μm is punched into the cell wall of the plant cell and fluorescently labelled DNA is forced into the cell by slight osmotic pressure differences. The uptake of the DNA is imaged by the fluorescence in a part of the cell in Fig. 22b. This direct transfer of DNA into plant cells is applicable for all cell types, and thus particularly crop plants can be genetically modified, in which other DNA transfer methods are only occasionally successful.

The possibility to work in the depth of a cell without opening it allows the study of the function of subcellular particles. For example, the mitotic spindle, the subcellular system which is responsible for accurate separation of chromosomes during cell division, can be inactivated by microbeam irradiation [66]. Since erroneous chromosome partition may be responsible for diseases such as mongolism (where chromosome 21 occurs in three instead of two copies), the laser microbeam may become an attractive tool to study the basic mechanism of these diseases. Furthermore, this technique is suitable for studying the mechanism of intracellular transport processes. For example, the cytoplasmic streaming is stopped by focussing a UV laser microbeam into the interior of a pollen tube and calcium is released from depots into the cytoplasm [71]. Studies are currently in progress to reveal the role of this calcium release in intracellular transport processes.

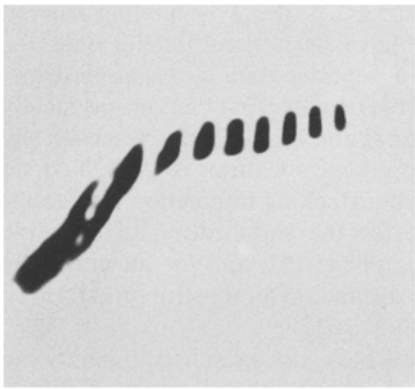

Fig. 23. Human chromosome dissected into slices of 300 nm using the diffraction rings of a laser microbeam

Figure 23 shows a human chromosome which is dissected into equal slices. For this experiment, diffraction, which is usually considered as an unwanted side effect of focussing to the theoretical limit, has been used to microdissect the chromosome. Microdissection is a basic technique used to study the molecular basis of disease. Many diseases such as muscular dystrophy, Alzheimer, cystic fibrosis, leukaemia and solid tumours are correlated with a defect in a specific region of a chromosome. In the past, the study of the molecular basis of such a disease took of the order of ten years, as in the case of the recently solved muscular dystrophy [73]. In those studies the portion of the *X* chromosome, which is defective in the disease, was isolated by sophisticated cell-biological methods. Laser microdissection promises to speed up that process by at least one order of magnitude, as is indicated in studies on the molecular basis of cystic fibrosis which are presently under way. With chromosomal material from the fruit fly drosophila, it has already been shown that the molecular-biological

techniques required for molecular analysis of disease can be applied to chromosome slices after laser microdissection [74].

Acknowledgements. Support of this work by the BMFT (TECFLAM, LABIO), DFG (SFB 123), Stiftung Volkswagenwerk, Fonds der Chemischen Industrie and the Commission of the European Communities is gratefully acknowledged. I also thank Dr. K. O. Greulich for compiling the section on biological applications of lasers.

References

1. F.P. Schäfer, W. Schmidt, J. Volze: Appl. Phys. Lett. **9**, 306 (1966)
   P.P. Sorokin, J.R. Lankard: IBM J. Res. Dev. **10**, 162 (1966)
2. F.P. Schäfer: Appl. Phys. B **46**, 197–206 (1988)
3. S. Arrhenius: Z. Physik. Chem. **4**, 226 (1889)
4. F. London: Z. Elektrochem. Angew. Phys. Chem. **35**, 592 (1929)
   P. Siegbahn, B. Liu: J. Chem. Phys. **68**, 2455 (1978); **80**, 581 (1984)
5. J. Arnold, D. Chandler, Th. Dreier: J. Chem. Phys. (to be published)
6. W. Meier, G. Ahlers, H. Zacharias: J. Chem. Phys. **85**, 2599 (1986)
7. Th. Dreier, J. Wolfrum: Int. J. Chem. Kinet. **18**, 919 (1986)
8. J. Wolfrum: Disc. Faraday Soc. **84** (1987)
9. U. Wellhausen, J. Wolfrum: Ber. Bunsenges. Phys. Chem. **89**, 314 (1985)
10. M. Kneba, J. Wolfrum: J. Phys. Chem. **83**, 69 (1979)
    D.K. Bondi, J.N.L. Connor, J. Manz, J. Römelt: Mol. Phys. **50**, 467 (1983)
11. K. Kleinermanns, J. Wolfrum: Angew. Chem. Int. Ed. Egl. **26**, 38 (1987)
12. D. Arnoldi, K. Kaufmann, J. Wolfrum: Phys. Rev. Lett. **34**, 1597 (1975)
13. J. Warnatz: Ber. Bunsenges. Phys. Chem. **87**, 1008 (1983)
    J. Wolfrum: 20th Symp. (Int.) on Combustion, The Combustion Institute (1984) p. 559
14. K. Kleinermanns, J. Wolfrum: J. Chem. Phys. **80**, 1446 (1984)
15. K. Kleinermanns, R. Schinke: J. Chem. Phys. **80**, 1440 (1984)
16. K. Kleinermanns, E. Linnebach: Appl. Phys. B **36**, 203 (1985)
17. I. Schechter, R.B. Bernstein, R.D. Levine: J. Phys. Chem. **91**, 5466 (1987)
18. J.A. Miller: J. Chem. Phys. **74**, 5120 (1981)
19. C.F. Melius, R.J. Blint: Chem. Phys. Lett. **64**, 183 (1979)
20. C. Cobos, H. Hippler, J. Troe: J. Phys. Chem. **89**, 342 (1985)
    J. Troe: J. Phys. Chem. **90**, 3485 (1986)
    J. Troe: Combust. Flame (1988) (in press)
21. T.H. Dunning, Jr., S.P. Walch, M.M. Goodgame: J. Chem. Phys. **74**, 3482 (1981)
22. G.J. Vazquez, S.G. Peyerimhoff, R.J. Buenker: Chem. Phys. **99**, 239 (1985)
23. G.L. Schott: Combust. Flame **21**, 357 (1973)
24. Th. Just, P. Frank: Ber. Bunsenges. Phys. Chem. **89**, 181 (1985)
25. A.N. Pirraglia, J.V. Michael, J.W. Sutherland, R.B. Klemm: J. Phys. Chem. (1988) (in press)
26. P.N. Clough, M. Kneba, M. Schneider, J. Wolfrum: Europäische Patentanmeldung Nr. 801056.490
27. M. Schneider, J. Wolfrum: Ber. Bunsenges. Phys. Chem. **90**, 1058 (1986)
28. A. Gupta, J.T. Yardley: Proc. SPIE Int. Soc. Opt. Eng. **458**, 131 (1984)
29. J. Kern, H. Schwahn, B. Schramm: Mat. Chem. Phys. (1988)
30. R.L. Whetten, K.J. Fu, E.R. Grant: J. Am. Chem. Soc. **104**, 4270 (1982)
31. J.C. Mitchener, M.S. Wrighton: J. Am. Chem. Soc. **103**, 975 (1981)
32. M. Gehring, K. Hoyermann, H. Schacke, J. Wolfrum: 14th Symp. (Int.) on Combustion, The Combustion Institute (1973) p. 99
33. Th. Dreier, J. Wolfrum: 20th Symp. (Int.) on Combustion, The Combustion Institute (1984) p. 695
34. R.K. Lyon: U. S. Patent Nr. 39.00.55.4
35. H. Hemberger, H. Neckel, J. Wolfrum: Third TECFLAM Seminar. Stuttgart (1987) p. 47
36. G. Damköhler: Z. Elektrochem. **46**, 601 (1940)
37. K.N.C. Bray, P.A. Libby: Phys. Fluids **19**, 1687 (1976)
38. H. Tsuji: Progr. Energy Combust. Sci. **8**, 93 (1982)
39. A.C. Eckbreth, G.M. Pobbs, J.H. Stufflebeam, P.A. Tellex: Appl. Opt. **23**, 1328 (1984)
40. R.J. Hall, L.R. Boedeker: Appl. Opt. **23**, 1340 (1984)
41. L.A. Rahn, L.J. Zych, F.L. Mattern: Opt. Commun. **30**, 249 (1979)
42. J.R. Hall, J.F. Verdieck, A.C. Eckbreth: Opt. Commun. **35**, 69 (1980)
43. D.A. Greenhalgh, R.J. Hall: Opt. Commun. **57**, 125 (1986)
44. R.E. Teets: Opt. Lett. **19**, 226 (1984)
45. M.A. Yuratich: Mol. Phys. **38**, 625 (1979)
46. M.H. Koszykowsky, R.L. Farrow, R.E. Palmer: Opt. Lett. **10**, 478 (1985)
47. A. Kim: J. Chem. Education **47**, 120 (1970)
48. G. Dixon-Lewis, T. David, P.H. Gaskell, S. Fukutani, H. Jinno, J.A. Miller, R.J. Kee, M.D. Smooke, N. Peters, E. Effelsberg, J. Warnatz, F. Behrendt: 20th Symp. (Int.) on Combustion, The Combustion Institute (1984) p. 1893
    Th. Dreier, B. Lange, J. Wolfrum, M. Zahn, F. Behrendt, J. Warnatz: Ber. Bunsenges. Phys. Chem. **90**, 1010 (1986)
    E. Dießel, Th. Dreier, B. Lange, J. Wolfrum, F. Behrendt, J. Warnatz: 22nd Symp. (Int.) on Combustion, The Combustion Institute (1988)
49. R.K. Hanson: 21st Symp. (Int.) on Combustion, The Combustion Institute (in press)
50. Z. Bor, B. Racz: Appl. Opt. **24**, 1910 (1985)
    F.P. Schäfer: Laser Optoelektron. **2**, 95 (1984)
51. Z. Bor: IEEE J. QE-**16**, 517 (1980)
    A. Müller, Z. Bor: Laser Optoelektron. **3**, 187 (1984)
52. S. Szatmari, Z. Bor: Appl. Phys. B **34**, 29 (1984)
53. R. Schwarzwald, P. Monkhouse, J. Wolfrum: Chem. Phys. Lett. **142**, 15 (1987)
54. H.M. Hertz, M. Alden: Appl. Phys. B **42**, 97 (1987)
55. L.D. Chen, W.M. Roquemore: Combust. Flame **66**, 81 (1986)
56. H. Becker, K. Kleinermanns, P. Monkhouse, R. Suntz, J. Wolfrum, J. Koehler, G. Ziegler: 22nd Symp. (Int.) on Combustion, The Combustion Institute (1988)
57. M. Noble, E.K.C. Lee: J. Chem. Phys. **80**, 134 (1984)
58. H.J. Polland, M.A. Franz, W. Zinth, W. Kaiser, E. Kölling, D. Oesterhelt: Biophys. J. **49**, 657 (1986)
59. J.E. Rudzki, K.S. Peters: Biochemistry **23**, 3843 (1984)
60. L. Stryer: Ann. Rev. Bioch. **47**, 819 (1978)
61. C. Helene, J.C. Maurizot: Crit. Rev. Bioch. **10**, 213–258 (1981)
62. K.O. Greulich, R.W. Wijnaendts van Resandt: Bioch. Bioph. Acta **782**, 446 (1984)
63. M.T. Record, C.F. Anderson, T.H. Lohmann: Q. Rev. Bioph. **11**, 103 (1978)

64. J. Ausio, K.O. Greulich, E. Haas, E. Wachtel: Biopolymers **23**, 2559 (1984)
65. K.O. Greulich, S. Monajembashi, T. Cremer, C. Cremer, P. Butz, J. Wolfrum: Proceedings of the CLEO, San Francisco (1986) p. 72
66. M.W. Berns, J. Aist, J. Edwards, K. Strahs, J. Girton, P. Mc Neill, J.B. Rattner, M. Kitzes, M. Hammer-Wilson, L.H. Liaw, A. Siemens, M. Koonce, S. Peterson, S. Brenner, J. Burt, R. Walter, P.J. Bryant, D.A. Van Dyk, J. Coulombe, T. Cahill, G.S. Berns: Science **213**, 505 (1981)
67. R. Wiegand, K. Zimmermann, S. Monajembashi, H. Schäfer, G.M. Hänsch, K.O. Greulich, J. Wolfrum: Immunobiology **173**, 320 (1986)
68. R. Wiegand, G. Weber, K. Zimmermann, S. Monajembashi, J. Wolfrum, K.O. Greulich: J. Cell Sci. **88**, 145 (1987)
69. G. Weber, S. Monajembashi, K.O. Greulich, J. Wolfrum: Naturwissenschaften **75**, 35 (1988)
70. S. Monajembashi, C. Cremer, T. Cremer, J. Wolfrum, K.O. Greulich: Exp. Cell. Res. **167**, 262 (1986)
71. H.D. Reiss, K.O. Greulich, J. Wolfrum, K. Zimmermann: Eur. J. Cell. Biol. (1988) (in press)
72. M.M.S. Lo, T.Y. Tsong, M.K. Konrad, S.M. Strittmater, L.D. Hesler, S.H. Snyder: Nature **310**, 792 (1984)
73. E.P. Hoffmann, R.H. Brown, Jr., L.M. Kunkel: Cell. **57**, 919 (1987)
74. N. Ponelies, E.K.F. Bautz, S. Monajembashi, J. Wolfrum, K.O. Greulich: Chromosoma (to be published) (1988)